ACS chemical biology

Letters

pubs.acs.org/acschemicalbiology

Micropattern-Controlled Local Microtubule Nucleation, Transport, and Mesoscale Organization

Surajit Ghosh,[†] Christian Hentrich,[‡] and Thomas Surrey*[,§]

Cell Biology and Biophysics Unit, European Molecular Biology Laboratory, Meyerhofstrasse 1, 69117 Heidelberg, Germany

Supporting Information

ABSTRACT: Microtubule organization in living cells is determined by spatial control of microtubule nucleation, their dynamic properties, and transport by molecular motors. Here, we establish a new micropattern-guided method for controlling local microtubule nucleation by spatially confined immobilization of a microtubule polymerase and show that these nucleated microtubules can be transported and organized in space by motor proteins. This assay provides a new platform for deciphering the principles underlying mesoscale microtubule organization.

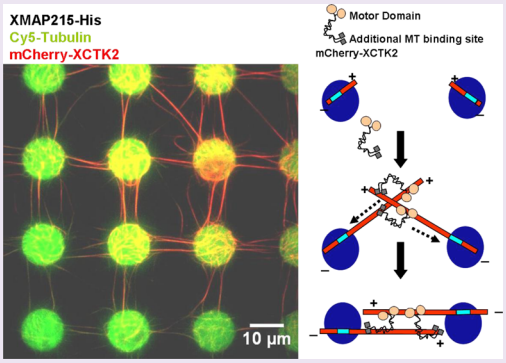

Eukaryotic cells have distinct internal architectures, reflecting their different biological tasks.[1] The intracellular organization is largely determined by the microtubule cytoskeleton. Microtubules are tube-like, structurally polar filaments composed of tubulin subunits. Microtubules typically switch between phases of growth and shrinkage, a property called dynamic instability.[2] In living cells, the dynamic properties of microtubules are controlled by a variety of regulatory proteins, which catalyze microtubule polymerization,[3] destabilize microtubules,[4] or help microtubules to regrow after depolymerization.[5] Additionally, local microtubule nucleation is a key control parameter for microtubule organization and, as such, is tightly regulated. In animal cells, microtubules are usually nucleated from specialized organelles called centrosomes[6] and, before cell division, often also around chromosomes.[7] Other activities determining the microtubule architecture are microtubule cross-linking proteins[8] and molecular motors.[7]

In vitro experiments with purified proteins have advanced our understanding of the properties of individual components of the cytoskeleton. Examples for classical motility assays include microtubule gliding assays in which preformed stabilized microtubules are transported by surface-immobilized motor proteins as well as single molecule assays in which individual processive motors are observed as they move along immobilized stabilized microtubules.[9,10] Motor proteins have generated interest for their usability in biotechnological applications, especially in combination with micropatterned immobilization of proteins or by immobilizing proteins in a microfabricated three-dimensional environment, however typically using stabilized, nondynamic microtubules.[11−16] Nonmotor proteins such as end tracking proteins of the EB family,[17] the polymerase XMAP215[3] or antiparallel microtubule bundling proteins[18,19] have been analyzed in experiments where dynamic microtubules grow from prepolymerized, stabilized, and randomly distributed immobilized microtubule fragments (seeds). Recently, microtubule seeds have also been immobilized on micropatterned or microfabricated substrates that could then be elongated in subsequent steps.[20,21]

Comparatively few *in vitro* studies have addressed directly the question of how the molecular components of the cytoskeleton self-organize dynamically in space. Early work has demonstrated that purified centrosomes nucleate microtubules *in vitro* in the presence of purified tubulin, forming aster-like structures.[22] More recently, the interaction of such asters with walls of microchambers mimicking the cell boundary were investigated.[23,24] An alternative pathway of microtubule aster formation is observed in mixtures of microtubule-cross-linking motors and tubulin. Here, microtubules nucleate uniformly in solution, grow, and are then focused into poles by motors.[25−27] It is however unclear how more complex microtubule organizations such as, for example, mitotic spindles are generated that require defined local nucleation of microtubules that can then be arranged in space by molecular motors.[7]

Here, with the aim to locally generate dynamic microtubules in predefined regions that can be transported by motor proteins, we produced micropatterns on glass surfaces that contained chemically functionalized areas on which the microtubule polymerase XMAP215[3] (a *Xenopus laevis* chTOG family member) was selectively immobilized. We first produced a micropattern of Ni-loaded Tris-(*nitrilo* tri-aceticacid)-polyethylene glycol (Tris-NTA-PEG) on a glass surface using a

Received: October 26, 2012
Accepted: January 7, 2013
Published: January 8, 2013

previously developed method[11] and then locally immobilized purified XMAP215 tagged with green fluorescent protein (GFP) and an oligo-histidine-sequence (XMAP215-GFP-His). His-tagged proteins bind essentially irreversibly to Tris-Ni-NTA-PEG functionalized surfaces.[28] Visualization by total internal reflection fluorescence (TIRF) microscopy revealed defined regions with high densities of immobilized XMAP215-GFP-His surrounded by PEG-passivated glass devoid of XMAP215 (Figure 1a). Binding was selective (Figure S1b, Supporting Information), and the protein density on Ni-Tris-NTA-PEG functionalized glass could be controlled by varying the protein concentration used for loading the Tris-Ni-NTA-PEG micropattern. Under our conditions, the density of immobilized protein was proportional to its concentration used for incubation (Figure S2a, Supporting Information). Compared to the smaller protein (His-GFP), the large XMAP215-GFP-His protein yielded lower number densities as expected.

To test the activity of immobilized XMAP215, which in its soluble form is known to bind unpolymerized tubulin,[3,29,30] we generated micropatterns with nonfluorescent XMAP215-His and added purified, Cy5-labeled tubulin (naturally lacking an oligo-histidine sequence). TIRF microscopy revealed that the fluorescent Cy5-tubulin bound selectively to the XMAP215-functionalized area (Figures 1b and S1c, Supporting Information), demonstrating that the immobilized XMAP215-His was active. Closer inspection revealed that in the presence of GTP, microtubules nucleated and grew from the XMAP215 surface area, but the high Cy5-tubulin fluorescence background in the XMAP215 area impeded clear visualization of these microtubules.

To overcome this problem, we added the microtubule end tracking protein Mal3 (the fission yeast EB1 homologue) that does not bind to soluble tubulin, but all along microtubules, and with a 10-fold increased affinity to growing microtubule end regions.[17,31] We observed that purified Mal3-GFP (lacking a His-tag) bound to dynamic microtubules as they were locally nucleated from XMAP215 areas on the surface and accumulated at both growing ends (Figure 1c). This demonstrates that fluorescently labeled Mal3 can be used as a highly selective marker for dynamic microtubules despite high tubulin densities on XMAP215-functionalized areas. These results demonstrate that locally controlled microtubule nucleation can be achieved by combining micropatterned chemical functionalization of glass and selective protein immobilization.

To better understand micropatterned microtubule nucleation, we tested how variation of several biochemical parameters affected the efficiency of nucleation. First, we increased the density of XMAP215-His on the functionalized Tris-Ni-NTA-PEG surface areas, and using Mal3-GFP as a microtubule marker, we observed an increasing microtubule density selectively on the XMAP215-functionalized areas (Figure 1d), demonstrating that XMAP215 effectively nucleates microtubules in a dose-dependent manner. The temporal behavior of individual freshly nucleated microtubules could be visualized in kymographs (time-space plots) (Figure 1e), demonstrating their characteristic dynamic nature. From more than 40 kymographs, we determined the mean growth velocities of the faster growing plus ends of microtubules nucleated locally from areas with different XMAP215-His densities. Thus, surface-immobilized XMAP215 accelerated tubulin growth in a dose-dependent manner (Figure 1f), as was previously reported for this microtubule polymerase when acting in

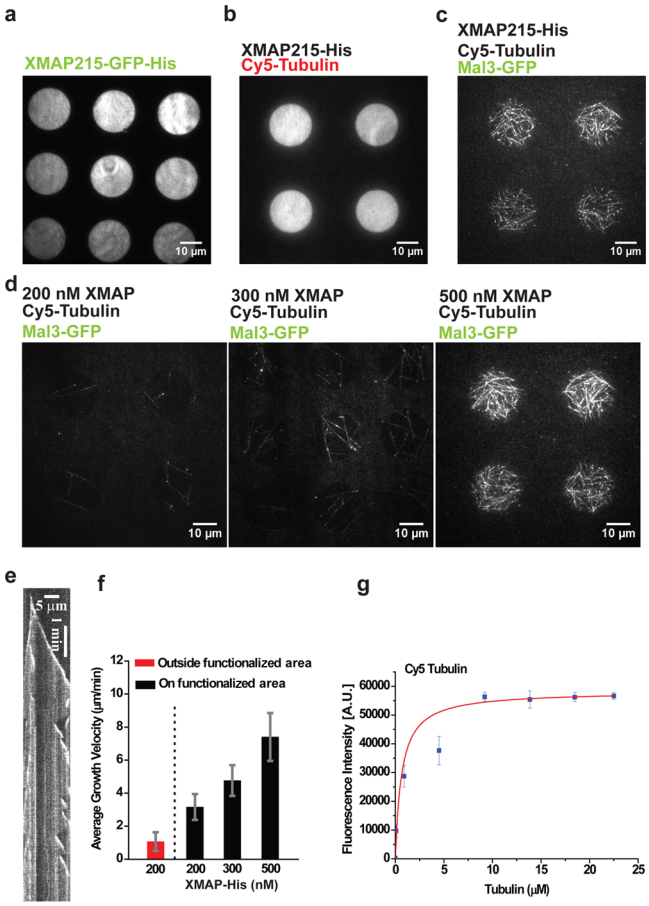

Figure 1. Patterned microtubule nucleation and efficiency of micropatterned microtubule nucleation. (a) TIRF microscopy image of fluorescent XMAP215-GFP-His immobilized on microfabricated Tris-Ni-NTA-PEG-functionalized glass areas (round patches). Concentration of XMAP215-GFP-His during the loading step was 500 nM. Image taken 5 min after immobilization of XMAP215-GFP-His. (b) TIRF microscopy image of Cy5-labeled tubulin bound to a XMAP215-functionalized micropattern 5 min after addition of Cy5-tubulin. Concentrations: 500 nM XMAP215-His during the immobilization step; 18.5 μM Cy-5 tubulin during imaging. (c) TIRF microscopy image of Mal3-GFP bound to dynamic microtubules that nucleated from a XMAP215-functionalized micropattern. Concentrations: 500 nM XMAP215-His during immobilization; 18.5 μM Cy-5 tubulin and 85 nM Mal3-GFP during imaging. Image taken 5 min after the addition of Mal3-GFP and Cy5-tubulin. (d) TIRF microscopy images showing Mal3-GFP labeled microtubules nucleated from XMAP215-His-functionalized micropatterns. Increasing the surface density by increasing the XMAP215-His concentration during immobilization (Figure S2b, Supporting Information), as indicated, increased the density of locally nucleated microtubules. Images taken 5 min after the addition of 85 nM Mal3-GFP and 18.5 μM Cy5-tubulin. (e) Example kymograph of a Mal3-GFP labeled nucleated microtubule on a XMAP215-functionalized micropattern. Loading concentration of XMAP215-His was 200 nM. (f) Graph of the average growth velocities of locally nucleated microtubules on functionalized patterns with different XMAP215 densities, as measured by TIRF microscopy. XMAP215-His concentrations used for loading as indicated. Red bar on the graph indicates the growth speed of nucleated microtubules outside the 200 nM XMAP215-His functionalized surface. (g) Average fluorescence intensity of Cy5-tubulin bound to XMAP215-functionalized micropatterns, as measured by TIRF microscopy, as a function of the Cy5-tubulin. The XMAP215-His concentration used for immobilization was 500 nM. The red line is a fit to the data using a hyperbolic function yielding a dissociation constant of 0.64 μM.

dx.doi.org/10.1021/cb300583p | ACS Chem. Biol. 2013, 8, 673−678

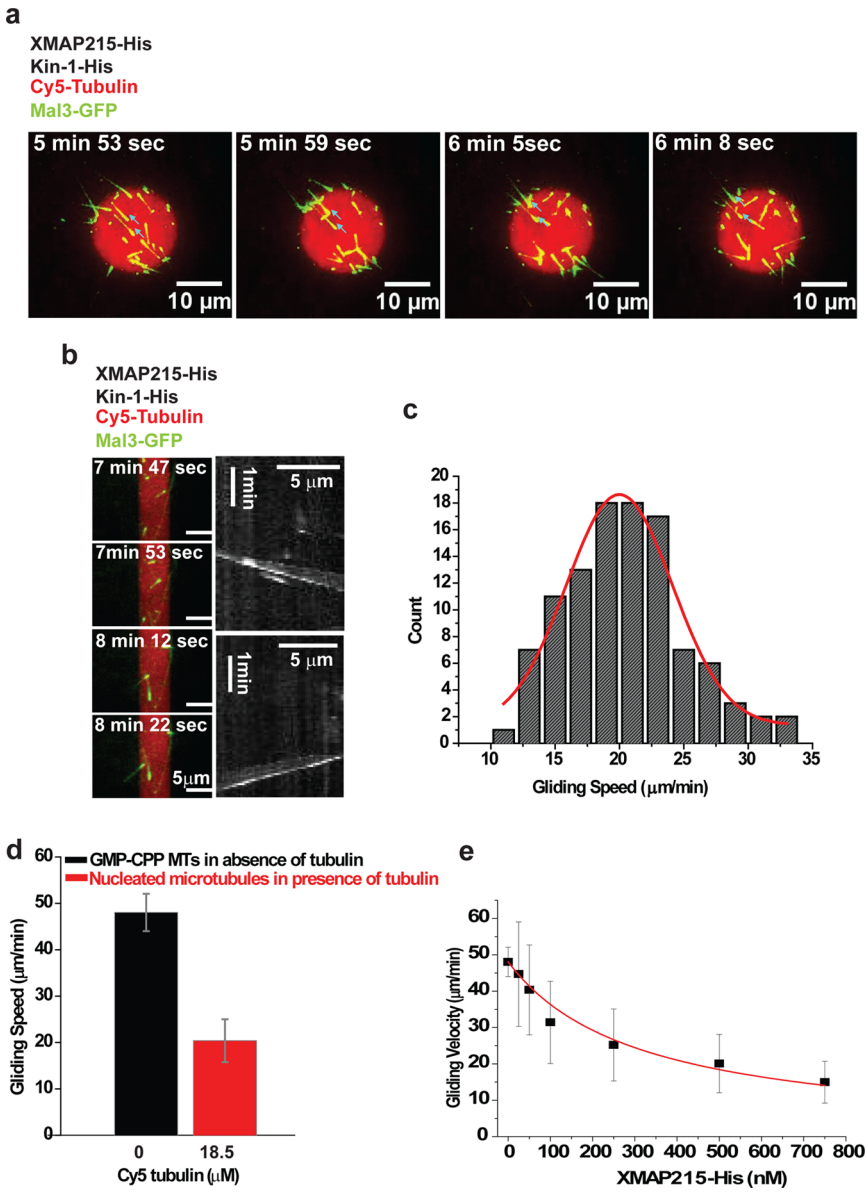

Figure 2. Motor protein mediated transport of locally nucleated microtubules. (a) Sequence of time-lapsed TIRF microscopy images showing Mal3-GFP-labeled microtubules (green) nucleated on a round XMAP215- and kinesin-1-double-functionalized area of a micropattern. Arrows point to two microtubules being transported by the immobilized motors from the center of the functionalized area to its periphery. Concentrations were 500 nM XMAP215-His and 50 nM kinesin-1-His for immobilization and 18.5 μM Cy5-tubulin (red) and 85 nM Mal3-GFP (green) during imaging. The indicated times are times after start of nucleation. (b) Left: Examples of freshly nucleated microtubules moving across a rectangular XMAP215- and kinesin-1-double-functionalized area of a micropattern. Right: Example kymographs of two freshly nucleated gliding Mal3-GFP microtubules as observed under conditions as in panel a. The tilted slope and the lateral widening of the microtubule signal indicate simultaneous directional motility and growth, respectively. (c) Histogram of gliding speeds of locally nucleated microtubules on micropatterns under conditions as in panel a. The red line shows a Gaussian fit to the data. (d) Graph with average gliding speeds of prepolymerized, GMP-CPP stabilized Cy5-microtubules on a glass with only immobilized kinesin-1-GFP (50 nM for loading) and of locally nucleated microtubules in the presence of 18.5 μM Cy5-tubulin and 85 nM Mal3-GFP on a glass with coimmobilized XMAP215-His (500 nM for loading) and kinesin-1-His (50 nM for loading). (e) Average gliding speeds of Cy5-labeled GMP-CPP-stabilized microtubules on micropatterns with constant kinesin-1-His densities (50 nM used for loading) and varying coimmobilized XMAP215-His densities. The red curve is a fit to the data using a model assuming protein friction exerted by the immobilized XMAP215 (see Methods).

solution.[3,32] This provides further evidence for immobilized XMAP215 having retained the characteristics of the soluble enzyme and shows that the growth velocity of surface-nucleated microtubules is affected by the presence of the immobilized polymerase.

The next parameter we measured was the effect of the tubulin concentration on local microtubule nucleation triggered by surface-immobilized XMAP215. First, we investigated how much Cy5-tubulin (measured by fluorescence intensity) was bound to XMAP215 micropattern-areas at different Cy5-tubulin concentrations and obtained a dissociation constant in the micromolar range (Figure 1g). This result agrees with previous qualitative determinations of XMAP215's binding activity.[29] We then monitored how the density of Mal3-GFP decorated microtubules nucleated from XMAP215-functionalized areas varied in response to the presence of different

dx.doi.org/10.1021/cb300583p | ACS Chem. Biol. 2013, 8, 673−678

tubulin concentrations. Interestingly, increasing the tubulin concentration in the regime of saturated tubulin binding to surface-immobilized XMAP215 still stimulated nucleation and/or microtubule stability (Figure S1a,d, Supporting Information). This demonstrates that, under our conditions, the efficiency of local microtubule generation is not limited by XMAP215's ability to catalyze microtubule polymerization.[3,29]

Next, we tested whether these locally nucleated microtubules could be transported by motor proteins. We coimmobilized both unlabeled XMAP215-His and unlabeled His-tagged kinesin-1 (kinesin-1-His), a plus-end directed motor protein,[33,34] on Tris-Ni-NTA-PEG areas of micropatterned glass and added Cy5-tubulin, GTP, ATP, and Mal3-GFP as a microtubule marker. We observed that locally nucleated and dynamic microtubules were indeed transported by the immobilized motors (Figure 2a). Kymographs of individual freshly nucleated microtubules demonstrated that these microtubules simultaneously elongated and moved (Figure 2b). The lagging microtubule plus end had typically more Mal3-GFP accumulated than the leading minus end, as expected.[17] The gliding speed was unimodally distributed, as is typical (Figure 2c). However, the mean velocity was significantly reduced by about 55% (Figure 2d, red bar) in comparison to the speed measured in a classical gliding assay. In such an assay, preformed microtubules were stabilized by the nonhydrolyzable GTP analogue GMP-CPP and were transported by immobilized kinesins in the absence of coimmobilized XMAP215 (Figure 2d, black bar).[33]

The slowdown of locally nucleated microtubules did not depend on the tubulin concentration (Figure S2b, Supporting Information). It was also not a characteristic feature of surface-nucleated microtubules in contrast to preformed microtubules because microtubules elongating from short GMP-CPP microtubules experienced a very similar tubulin concentration-independent slowdown on mixed kinesin-1-His/XMAP215-His surfaces (Figure S2c, Supporting Information). Instead, the reduction of the transport velocity could be demonstrated to depend on the density of surface-immobilized XMAP215 (Figure 2e). XMAP215 is known to not only bind soluble tubulin but also all along microtubules.[29] This slowdown is therefore most likely due to protein friction[35] generated when motors transport microtubules over an XMAP215 surface. Supporting this hypothesis, a model assuming protein friction could be well fitted to the data (Figure 2e, red curve). In controls, we showed that the surface density of the immobilized oligo-histidine-tagged motor was not affected by immobilizing increasing amounts of XMAP215-GFP-His (Figure S2d,e, Supporting Information) or GFP-His (Figure S2f, Supporting Information). These experiments represent the first microtubule gliding assays with locally nucleated and dynamic microtubules. They further support our previous conclusion that microtubules locally nucleated in XMAP215 areas are fully functional and show that the density of surface-immobilized microtubule binding proteins is a convenient control parameter for the speed of locally nucleated microtubules.

Finally, we combined local XMAP215 pattern-controlled microtubule nucleation with motor-microtubule self-organization. Microtubule cross-linking and sliding motors can organize microtubules in solution.[25−27] Here, we have shown that local nucleation centers can also control the spatial arrangement of microtubules. To test the outcome of the combination of both spatial organization strategies, we immobilized XMAP215-His on Tris-Ni-NTA-PEG micropatterns and added an mCherry-labeled microtubule minus-end directed microtubule cross-linking motor (*Xenopus* kinesin-14 XCTK2 that did not carry a His-tag). We observed that the soluble motor colocalized with the nucleated microtubules, serving in this experiment also as microtubule marker, and connected microtubules growing beyond different nucleation zones (Figure 3a). This resulted

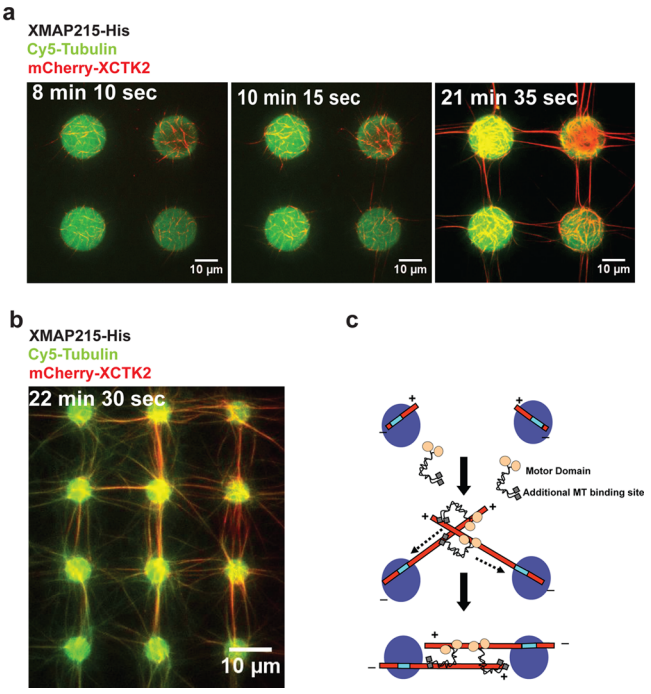

Figure 3. Motor protein-mediated large-scale organization of micropattern-nucleated microtubules. (a) Sequence of time-lapsed TIRF microscopy images of large-scale organization of microtubules that nucleate locally from a XMAP215-functionalized micropattern in the presence of 100 nM of the soluble minus end-directed microtubule-cross-linking and sliding motor mCherry-kinesin-14 (red) and 18.5 μM Cy5-tubulin (green). Microtubules are visualized by the bound mCherry-tagged motor, and the XMAP215-functionalized areas are visualized by bound Cy5-tubulin. Loading concentration of XMAP215-His for immobilization was 500 nM. Times after start of the experiment are indicated. (b) TIRF microscopy image of a larger area of an mCherry-kinesin-14 organized network of microtubules that were locally nucleated from a XMAP215-functionalized micropattern as observed under conditions as in panel a. The image was taken 20 min after the start of nucleation. (c) Schematic of the molecular mechanism leading to the large scale-network in panels a and b. The cyan part of the otherwise red microtubule indicates an imaginary fiduciary mark.

in regular patterns of bundled, straight microtubules connecting all nucleation zones preferentially along their shortest distance (Figure 3b). The emergence of this remarkable microtubule architecture was indicative of motor-mediated pulling forces straightening the bundles. This is plausible as microtubule plus-ends grow faster than minus-ends and therefore tend to meet first when microtubules encounter each other between nucleation centers. Minus-end directed cross-linking kinesin-14 motors are then expected to pull on such connections by walking along microtubules toward the nucleation zones, thereby stretching the interconnected bundles (Figure 3c). Coimmobilizing kinesin-1-His with XMAP215-His leads to the opposite microtubule orientation (microtubules being transported out of the functionalized areas with their minus ends

dx.doi.org/10.1021/cb300583p | *ACS Chem. Biol.* 2013, 8, 673−678

leading), which does not allow kinesin-14 to establish a regular mesoscale microtubule organization (Figure S3, Supporting Information).

In conclusion, our experiments have demonstrated that several complementary strategies can be combined to organize microtubules in space *in vitro*. Prestructuring a surface with a chemical functionalization that affords selective immobilization of a microtubule nucleating protein allows the design of defined nucleation centers determining where microtubules are produced. Coimmobilized microtubule motors transport locally nucleated, dynamic microtubules, whereas soluble microtubule cross-linking motors cause mesoscale microtubule organization connecting microtubules growing beyond nucleation centers. The new experimental system described here and a complementary assay recently developed for actin filament networks[36] allow the systematic study of the interplay between spatially preorganized biomechanically active proteins and self-organizing molecules in solution. These types of experiments promise to lead to a better understanding of complex cytoskeleton organizations by allowing the systematic exploration of the biochemical and physical parameter spaces of reconstituted cytoskeleton systems.

METHODS

Local Microtubule Nucleation on Functionalized Micropatterns. A flow chamber of around 5 μL was built from one glass with a Ni-loaded micropattern of Tris-NTA-PEG functionalization (patterned glass) and one poly-L-lysine (PLL)-PEG passivated counter glass, separated by two strips of double sticky tape (Tesa, Hamburg, Germany).[10,11] The flow chamber was equilibrated with 20 μL of BRB80 (80 mM PIPES, 1 mM EGTA, 1 mM $MgCl_2$ pH 6.8) while positioned on an ice-cold metal block, then with 20 μL of BRB80 containing 1 mg mL^{-1} β-casein for 5 min. Next, XMAP215-His_7 (200, 300, or 500 nM) was flowed into the flow chamber, followed by incubation for 10 min. Unbound XMAP215-His_7 was washed out by BRB80 supplemented with 300 mM KCl. Then, the flow chamber was filled with Cy5 tubulin (13% labeling ratio of Cy5 per tubulin; 9.25, 13.85, 18.5, or 23.07 μM) and 85 nM Mal3-EGFP in nucleation buffer (BRB80 supplemented with 3 mM GTP, 14.5 mM $MgCl_2$, and an oxygen scavenger system (50 mM glucose, 1 mg mL^{-1} glucose oxidase, and 0.5 mg mL^{-1} catalase)) on an ice cold metal block and transferred to the TIRF microscope. Time-lapse imaging was performed at 32 °C.

Motor-Mediated Transport of Locally Nucleated Microtubules on Functionalized Micropatterns. A flow chamber was prepared with one patterned and one passivated glass and the functionalized patches of the patterned surface were loaded with XMAP215-His_7 by incubating with 500 nM XMAP215-His_7, as described for the nucleation assay. Then, 50 nM Kin612-His_{10} in BRB80 was flowed into the chamber followed by 10 min incubation and then washing out with BRB80 supplemented with 300 mM KCl. The flow chamber was then filled with 18.5 μM Cy5 tubulin, 85 nM Mal3-EGFP, and 3 mM Mg-ATP in nucleation buffer and imaged by TIRF microscopy at 32 °C.

Motor-Mediated Large-Scale Organization of Microtubules Nucleated from Functionalized Micropatterns. For large-scale microtubule organization experiments (Figure 3), a micropattern (part of a flow chamber) of Ni-loaded Tris-NTA-PEG areas was loaded with 500 nM XMAP215-His_7 as described above and was finally filled with 18.5 μM Cy5-tubulin and 100 nM mCherry-XCTK2 in a nucleation buffer supplemented with 3 mM Mg-ATP. For control experiments, the functionalized areas were additionally loaded by incubation with 50 nM Kin612-His_{10} as described above. Local nucleation and large-scale organization was observed by time-lapse TIRF microscopy at 32 °C.

ASSOCIATED CONTENT

Supporting Information

Additional methods. This material is available free of charge via the Internet at http://pubs.acs.org.

AUTHOR INFORMATION

Corresponding Author

*E-mail: thomas.surrey@cancer.org.uk.

Present Addresses

[†]Chemistry Division, CSIR-Indian Institute of Chemical Biology, 4, Raja S.C. Mullick Road, Kolkata 700 032, India.
[‡]Massachusetts General Hospital, 185 Cambridge St., Boston, MA 02114, United States.
[§]Cancer Research U.K. London Research Institute, 44 Lincoln's Inn Fields, London, WC2A 3LY, U.K.

Notes

The authors declare no competing financial interest.

ACKNOWLEDGMENTS

We thank J. Seiler and E. Boutant for help during the expression of XMAP215 and S. Maurer and I. Telly for help during the analysis of data. We thank P. Widlund for the XMAP215-GFP-His plasmid. We thank F. J. Fourniol and J. Roostalu for critically reading the manuscript. S.G. was supported by a Humboldt fellowship. T.S. acknowledges support from the European Commission (FP6 STREP Active Biomics), the German Ministry of Education and Research (BMBF), and the German Research Foundation (DFG).

REFERENCES

(1) Keating, T. J., and Borisy, G. G. (1999) Centrosomal and non-centrosomal microtubules. *Biol. Cell 91*, 321−329.
(2) Mitchison, T., and Kirschner, M. (1984) Dynamic instability of microtubule growth. *Nature 312*, 237−242.
(3) Brouhard, G. J., Stear, J. H., Noetzel, T. L., Al-Bassam, J., Kinoshita, K., Harrison, S. C., Howard, J., and Hyman, A. A. (2008) XMAP215 is a processive microtubule polymerase. *Cell 132*, 79−88.
(4) Desai, A., Verma, S., Mitchison, T. J., and Walczak, C. E. (1999) Kin I kinesins are microtubule-destabilizing enzymes. *Cell 96*, 69−78.
(5) Al-Bassam, J., Kim, H., Brouhard, G., van Oijen, A., Harrison, S. C., and Chang, F. (2010) CLASP promotes microtubule rescue by recruiting tubulin dimers to the microtubule. *Dev. Cell 19*, 245−258.
(6) Barenz, F., Mayilo, D., and Gruss, O. J. (2011) Centriolar satellites: busy orbits around the centrosome. *Eur. J. Cell Biol. 90*, 983−989.
(7) Walczak, C. E., and Heald, R. (2008) Mechanisms of mitotic spindle assembly and function. *Int. Rev. Cytol. 265*, 111−158.
(8) Roostalu, J., Schiebel, E., and Khmelinskii, A. (2010) Cell cycle control of spindle elongation. *Cell Cycle 9*, 1084−1090.
(9) Yanagida, T., Iwaki, M., and Ishii, Y. (2008) Single molecule measurements and molecular motors. *Philos. Trans. R. Soc. London, Ser. B 363*, 2123−2134.
(10) Bieling, P., Telley, I. A., Hentrich, C., Piehler, J., and Surrey, T. (2010) Fluorescence microscopy assays on chemically functionalized surfaces for quantitative imaging of microtubule, motor, and +TIP dynamics. *Methods Cell Biol. 95*, 555−580.
(11) Bhagawati, M., Ghosh, S., Reichel, A., Froehner, K., Surrey, T., and Piehler, J. (2009) Organization of motor proteins into functional micropatterns fabricated by a photoinduced Fenton reaction. *Angew. Chem., Int. Ed. 48*, 9188−9191.
(12) Dinu, C. Z., Chrisey, D. B., Diez, S., and Howard, J. (2007) Cellular motors for molecular manufacturing. *Anat. Rec. 290*, 1203−1212.

(13) Korten, T., Mansson, A., and Diez, S. (2010) Towards the application of cytoskeletal motor proteins in molecular detection and diagnostic devices. *Curr. Opin. Biotechnol. 21*, 477−488.
(14) van den Heuvel, M. G., and Dekker, C. (2007) Motor proteins at work for nanotechnology. *Science 317*, 333−336.
(15) Doot, R. K., Hess, H., and Vogel, V. (2006) Engineered networks of orineted microtubule filaments for directed cargo transport. *Soft Matter 3*, 349−356.
(16) Roos, W., Ulmer, J., Grater, S., Surrey, T., and Spatz, J. P. (2005) Microtubule gliding and cross-linked microtubule networks on micropillar interfaces. *Nano Lett. 5*, 2630−2634.
(17) Bieling, P., Laan, L., Schek, H., Munteanu, E. L., Sandblad, L., Dogterom, M., Brunner, D., and Surrey, T. (2007) Reconstitution of a microtubule plus-end tracking system *in vitro*. *Nature 450*, 1100−1105.
(18) Bieling, P., Telley, I. A., and Surrey, T. (2010) A minimal midzone protein module controls formation and length of antiparallel microtubule overlaps. *Cell 142*, 420−432.
(19) Janson, M. E., Loughlin, R., Loïodice, I., Fu, C., Brunner, D., Nédélec, F. J., and Tran, P. T. (2007) Crosslinkers and motors organize dynamic microtubules to form stable bipolar arrays in fission yeast. *Cell 128*, 357−368.
(20) Portran, D., Gaillard, J., Vantard, M., and Thery, M. (2012) Quantification of MAP and molecular motor activities on geometrically controlled microtubule networks. *Cytoskeleton,*.
(21) Uppalapati, M., Huang, Y. M., Aravamuthan, V., Jackson, T. N., and Hancock, W. O. (2011) ″Artificial mitotic spindle″ generated by dielectrophoresis and protein micropatterning supports bidirectional transport of kinesin-coated beads. *Integr. Biol. 3*, 57−64.
(22) Mitchison, T., and Kirschner, M. (1984) Microtubule assembly nucleated by isolated centrosomes. *Nature 312*, 232−237.
(23) Faivre-Moskalenko, C., and Dogterom, M. (2002) Dynamics of microtubule asters in microfabricated chambers: the role of catastrophes. *Proc. Natl. Acad. Sci. U.S.A. 99*, 16788−16793.
(24) Laan, L., Pavin, N., Husson, J., Romet-Lemonne, G., van Duijn, M., López, M. P., Vale, R. D., Jülicher, F., Reck-Peterson, S. L., and Dogterom, M. (2012) Cortical dynein controls microtubule dynamics to generate pulling forces that position microtubule asters. *Cell 148*, 502−514.
(25) Hentrich, C., and Surrey, T. (2010) Microtubule organization by the antagonistic mitotic motors kinesin-5 and kinesin-14. *J. Cell Biol. 189*, 465−480.
(26) Nedelec, F. J., Surrey, T., Maggs, A. C., and Leibler, S. (1997) Self-organization of microtubules and motors. *Nature 389*, 305−308.
(27) Surrey, T., Nedelec, F., Leibler, S., and Karsenti, E. (2001) Physical properties determining self-organization of motors and microtubules. *Science 292*, 1167−1171.
(28) Lata, S., and Piehler, J. (2005) Stable and functional immobilization of histidine-tagged proteins via multivalent chelator headgroups on a molecular poly(ethylene glycol) brush. *Anal. Chem. 77*, 1096−1105.
(29) Widlund, P. O., Stear, J. H., Pozniakovsky, A., Zanic, M., Reber, S., Brouhard, G. J., Hyman, A. A., and Howard, J. (2011) XMAP215 polymerase activity is built by combining multiple tubulin-binding TOG domains and a basic lattice-binding region. *Proc. Natl. Acad. Sci. U.S.A. 108*, 2741−2746.
(30) Ayaz, P., Ye, X., Huddleston, P., Brautigam, C. A., and Rice, L. M. (2012) A TOG:alphabeta-tubulin complex structure reveals conformation-based mechanisms for a microtubule polymerase. *Science 337*, 857−860.
(31) Maurer, S. P., Bieling, P., Cope, J., Hoenger, A., and Surrey, T. (2011) GTPgammaS microtubules mimic the growing microtubule end structure recognized by end-binding proteins (EBs). *Proc. Natl. Acad. Sci. U.S.A. 108*, 3988−3993.
(32) Gard, D. L., and Kirschner, M. W. (1987) A microtubule-associated protein from Xenopus eggs that specifically promotes assembly at the plus-end. *J. Cell Biol. 105*, 2203−2215.
(33) Bieling, P., Telley, I. A., Piehler, J., and Surrey, T. (2008) Processive kinesins require loose mechanical coupling for efficient collective motility. *EMBO Rep. 9*, 1121−1127.
(34) Vale, R. D., Schnapp, B. J., Mitchison, T., Steuer, E., Reese, T. S., and Sheetz, M. P. (1985) Different axoplasmic proteins generate movement in opposite directions along microtubules *in vitro*. *Cell 43*, 623−632.
(35) Tawada, K., and Sekimoto, K. (1991) Protein friction exerted by motor enzymes through a weak-binding interaction. *J. Theor. Biol. 150*, 193−200.
(36) Reymann, A. C., Boujemaa-Paterski, R., Martiel, J. L., Guérin, C., Cao, W., Chin, H. F., De La Cruz, E. M., Théry, M., and Blanchoin, L. (2012) Actin network architecture can determine myosin motor activity. *Science 336*, 1310−1314.

NOTE ADDED AFTER ASAP PUBLICATION

This paper was published ASAP on January 14, 2013. The Supporting Information file has been updated. The revised version posted on March 4, 2013.